Coupled Systems Mechanics, *Vol. 14, No. 1 (2025) 21-42*
https://doi.org/10.12989/csm.2025.14.1.021

Axisymmetric forced vibration of the elastic plate in contact with a compressible viscous fluid layer

Surkay D. Akbarov*[1,2], Jamila N. Imamaliyeva[3a] and Zafer Kutug[4b]

[1]*Department of Mechanical Engineering, Faculty of Mechanical Engineering, Yildiz Technical University, Yildiz Campus, 3349, Besiktas, Istanbul, Turkiye*
[2]*Institute of Mathematics and Mechanics of Science and Education Ministry Republic of Azerbaijan, Baku, Az141, Azerbaijan*
[3]*Azerbaijan University of Architecture and Construction, Baku, Az141, Azerbaijan*
[4]*Department of Civil Engineering, Faculty of Civil Engineering, Yildiz Technical University, 34220, Istanbul, Turkiye*

(Received May 12, 2024, Revised February 5, 2025, Accepted February 7, 2025)

Abstract. The paper studies the axisymmetric frequency response of the hydro-elastic system consisting of an elastic plate, barotropic compressible viscous fluid, and rigid wall under the action on the plate a point-located time-harmonic force. The motion of the plate is described by utilizing the exact equations of linear elastodynamics. The fluid flow is defined by the linearized Navier-Stokes equations for compressible viscous fluids. For the solution to the problem, the Hankel integral transform is employed and the transforms for the sought quantities are found analytically from the solution of the corresponding field equations. The inverse of these transforms is found numerically by employing the corresponding algorithms and PC programs. Numerical results are presented for the frequency response of the normal stress (pressure) on the interface plane between the fluid and plate. In obtaining these results, it is assumed that the plate material is steel or Lucite, however, Glycerin or water is taken as the fluid. Based on these results, the influence of the problem parameters, such as fluid viscosity, fluid depths, and vibration phase on these frequency responses under various plate thicknesses is studied.

Keywords: axisymmetric forced vibration; compressible viscous fluid; fluid depth; frequency response; plate+fluid hydro-elastic system; resonance frequencies

1. Introduction

The study of the dynamics of plate-fluid hydro-elastic systems has great significance in the theoretical and application sense in aerospace, nuclear, naval, chemical, and biomedical engineering. These studies were started by Lamb (1921) in which vibrations of a circular elastic "baffled" plate in contact with still water are considered. Since then, these investigations have

*Corresponding author, Professor, E-mail: akbarov@yildiz.edu.tr
[a]Associate Professor, E-mail: ncamila@rambler.ru
[b]Associate Professor, E-mail: kutug@yildiz.edu.tr

http://www.techno-press.org/?journal=csm&subpage=8 ISSN: 2234-2184 (Print), 2234-2192 (Online)

been further developed in many studies, which can be conditionally divided into two groups: Studies related to wave propagation and the free vibration of the system belong to the first group, while studies related to the forced vibration of the system belong to the second group. A review of the first group of investigations is detailed in the papers (Guz and Bagno 2018, 2019, Akbarov and Negin 2021, 2022, Akbarov and Bagirov 2022, 2023, Cao *et al.* 2024, Ulbricht *et al*. 2024) while a review of the second group of investigations is detailed in the papers (Akbarov 2018, Paimushin and Gazizullin 2021, Paimushin *et al*. 2020, Koçal 2021, Taati *et al*. 2024) and many others listed therein. We also refer to the vibration analysis of the plate resting on the elastic foundations carried out in the works of Abdulbaki *et al.* (2022), Hadji *et al*. (2021) and other works cited therein.

It follows from the mentioned above review papers and from the above brief review that these investigations can also be classified as to the accuracy of the applied plate theories and with respect to the models used in describing the fluid flow.

As usual, to simplify the study of the related mathematical problems, the motion of the plate is described within the framework of various approximate plate theories, and the fluid is modeled as an incompressible inviscid one. As examples of more recent studies that were made by the approximate plate theories, are the works (Askari *et al*. 2020, Popov *et al*. 2024, Wu *et al*. 2023, Iurlov *et al.* 2022) and others listed in these works. Consider a brief review of these works and begin this review with the paper (Askari *et al*. 2020) which deals with the development of an approximate analytical method to study the fluid-coupled vibration of eccentric annular plates. The motion of the plate is described using Kirchhoff's plate theories, but the flow of the fluid is described within the incompressible, non-viscous fluid model.

The paper (Popov *et al*. 2024) investigates the nonlinear oscillation of a plate resting on a nonlinear Winkler foundation. The motion of the plate is described by Kirchhoff's plate theory and it is assumed that the response of the elastic foundation to the lateral deflection of the plate exhibits a cubic nonlinearity. At the same time, it is assumed that the plate forms the bottom of the channel filled with the viscous gas and that the upper channel wall is rigid. The flow of the gas is described by the two-dimensional Navier-Stokes equations for a barotropic compressible medium. It is assumed that the law of pressure pulsation is given at the ends of the channel. An attempt is made to determine the response of the plate to this pulsation of pressure.

Small amplitude waves in a floating poroelastic plate forced by a vertical pitching plate are investigated in the paper (Wu *et al*. 2023). In this study, a hydroelastic system consisting of the plate, an incompressible, inviscid fluid layer and a rigid wall that restricts the flow of the fluid is considered. The movement of the plate is described by Kirchhoff theory.

The experimental investigation of the effects of the height of the liquid layer, the viscosity of the liquid and the free surface waves on the vibration damping of the rectangular plate in contact with this layer is carried out in the paper (Iurlov *et al*. 2022).

It is obvious that although such approaches simplify the solution procedure, they cannot describe many dynamic effects such as the dispersion of waves, the length of which is comparable with the plate thickness. In addition, these approximate theories cannot take into consideration the influence of fluid compressibility and viscosity on the pressure and velocity distribution of the fluid under forced vibration plate+fluid systems. However, by employing the so-called exact three-dimensional linearized Navier-Stokes equations for describing the fluid flow, and the three-dimensional linearized equations of elastodynamics for describing the plate motion for the study of the dynamics of the plate+fluid systems, we obtain results that take into account all the above features of the studied problems which can be taken as the benchmarks for the corresponding

results of any approximate theories. Examples of the aforementioned works related to the first group and carried out within the framework of exact equations and relations can be taken from the studies made in the papers (Akbarov and Negin 2021, 2022, Akbarov and Bagirov 2022, 2023, Bagno 2017a, 2017b, 2019, Guz and Bagno 2017, 2018, 2019) and others listed in these papers.

However, to the best of the authors' knowledge, from the historical aspect, the works related to the second group and carried out within the scope of the exact equations and relations mentioned above only started recently, and the first considerable results in this field are detailed in the papers (Akbarov and Ismailov 2016, 2017). These investigations were developed in the paper (Akbarov and Ismailov 2018) for the case where the plate material is viscoelastic and developed in the paper (Akbarov and Huseynova 2019) for the case where the plate material is orthotropic. At the same time, the corresponding results for the PZT plate and metal+PZT plate were obtained in the papers (Ekicioglu Kuzeci and Akbarov 2023a, b). The results, which are similar to those obtained in the paper (Akbarov and Ismailov 2016), are also discussed in the monograph (Akbarov 2015). There are other related investigations, which are reviewed in the paper (Akbarov 2018).

In the investigations related to the second group, the hydro-elastic system is modeled as an infinite plate+infinite compressible viscous fluid layer+rigid wall restricting the fluid flow. Within this modeling, the forced vibration of the plate+fluid hydro-elastic system is studied for the case where harmonic lineally-located forces act on the plate, i.e., it is assumed that the plane strain state occurs in the plate, and the plane flow occurs in the fluid layer. The results obtained within these assumptions cannot be applied to the cases where the point-located forces or the forces located in a finite region of the face plane act on the plate. In general, to obtain results related to the point-located forces case, solving the corresponding three-dimensional problems is necessary, which is more complicated than those related to the plane-strain state. However, as the first step in this field, the corresponding axisymmetric forced vibration case caused by the point-located axisymmetric forces acting on the plate can be considered. Namely, this axisymmetric problem is studied in the present paper for the hydro-elastic system consisting of the plate, compressible viscous fluid, and rigid wall. In this study, the motion of the plate is described by the exact equations of linear elastodynamics and the fluid flow by the linearized Navier-Stokes equations.

2. Formulation of the problem

Consider a hydro-elastic system consisting of the elastic plate-layer, barotropic compressible Newtonian viscous fluid, and rigid wall, the sketch of which is illustrated in Fig. 1. We associate the cylindrical system of coordinates $Or\theta z$ and Cartesian system of coordinates $Ox_1x_2x_3$ with the upper face plane of the plate. According to the selected coordinate systems and to Fig. 1, the plate occupies the region $\{0 \le r < \infty, 0 \le \theta \le 2\pi, -h \le z \le 0\}$, but the fluid occupies the region $\{0 \le r < \infty, 0 \le \theta \le 2\pi, -h_d \le z \le h\}$. Then, we consider the plate's motion where the point-located normal time-harmonic force acts on its free face plane, and this plate is in contact with the compressible viscous fluid layer, the flow of which is restricted with the rigid wall (Fig. 1).

Thus, according to the preceding statements, in the hydro-elastic system under consideration, the axisymmetric state in the cylindrical system of coordinates $Or\theta z$ appears, and the following equations of motion for the plate can be written

$$\frac{\partial Q_{rr}}{\partial r}+\frac{\partial Q_{zr}}{\partial z}+\frac{1}{r}\left(Q_{rr}-Q_{\theta\theta}\right)=\rho\frac{\partial^2 u_r}{\partial t^2},\ \frac{\partial Q_{rz}}{\partial r}+\frac{\partial Q_{zz}}{\partial z}+\frac{1}{r}Q_{rz}=\rho\frac{\partial^2 u_z}{\partial t^2}, \tag{1}$$

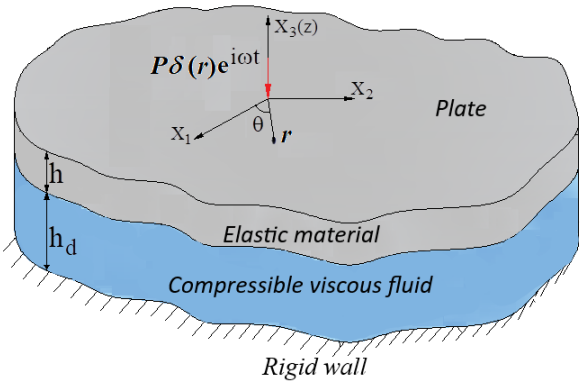

Fig. 1 Sketch of the hydro-elastic system

where $Q_{rr}, Q_{rz}, \ldots, Q_{zz}$ are the components of the stress tensor in the plate, u_r and u_z are the components of the displacement vector, and ρ is the plate material density.

Also, we write the elasticity relations for the plate material

$$Q_{rr} = (\lambda + 2\mu)\frac{\partial u_r}{\partial r} + \lambda\frac{u_r}{r} + \lambda\frac{\partial u_z}{\partial z},\ Q_{\theta\theta} = (\lambda + 2\mu)\frac{u_r}{r} + \lambda\frac{\partial u_r}{\partial r} + \lambda\frac{\partial u_z}{\partial z},$$
$$Q_{zz} = (\lambda + 2\mu)\frac{\partial u_z}{\partial z} + \lambda\frac{u_r}{r} + \lambda\frac{\partial u_r}{\partial r},\ Q_{rz} = \mu\left(\frac{\partial u_r}{\partial z} + \frac{\partial u_z}{\partial r}\right), \tag{2}$$

where λ and μ are the Lame's constants.

This completes the writing of the field equations for the plate motion.

Now we consider the linearized Navier-Stokes equations describing the flow of the barotropic compressible viscous fluid. These equations in terms of the velocities are

$$\rho_{01}\frac{\partial}{\partial t}V_r = \mu^{(1)}\left(\frac{\partial^2}{\partial r^2}V_r + \frac{1}{r}\frac{\partial}{\partial r}V_r + \frac{\partial^2}{\partial z^2}V_r - \frac{1}{r^2}V_r\right) + (\lambda^{(1)} + \mu^{(1)})\frac{\partial}{\partial r}\left(\frac{\partial(rV_r)}{r\partial r} + \frac{\partial V_z}{\partial z}\right) - \frac{\partial}{\partial r}p_1,$$
$$\rho_{01}\frac{\partial}{\partial t}V_z = \mu^{(1)}\left(\frac{\partial^2}{\partial r^2}V_z + \frac{1}{r}\frac{\partial}{\partial r}V_z + \frac{\partial^2}{\partial z^2}V_z\right) + (\lambda^{(1)} + \mu^{(1)})\frac{\partial}{\partial z}\left(\frac{\partial(rV_r)}{r\partial r} + \frac{\partial V_z}{\partial z}\right) - \frac{\partial}{\partial z}p_1 \tag{3}$$

where ρ_{01} is the fluid density before the perturbation, $\lambda^{(1)}$ and $\mu^{(1)}$ are the coefficients of the fluid viscosity, p_1 is the perturbation of the pressure, V_r, and V_z are the components of the perturbation velocity vector. We add to equations in (3) the continuity and state equations, and rheological relations.

The continuity equation

$$\frac{\partial\rho_1}{\partial t} + \rho_{01}\left(\frac{\partial V_r}{\partial r} + \frac{V_r}{r} + \frac{\partial V_z}{\partial z}\right) = 0 \tag{4}$$

The state equation

$$p_1 = a_0^2\rho_1,\ a_0^2 = \left(\frac{\partial p_1}{\partial\rho_1}\right)_0 \tag{5}$$

The rheological relations

$$T_{rr} = -p_1 + \lambda^{(1)} e + 2\mu^{(1)} \frac{\partial V_r}{\partial r}, \; T_{\theta\theta} = -p_1 + \lambda^{(1)} e + 2\mu^{(1)} \frac{V_r}{r}, \quad T_{zz} = -p_1 + \lambda^{(1)} e + 2\mu^{(1)} \frac{\partial V_z}{\partial z},$$
$$T_{rz} = \mu^{(1)} \left(\frac{\partial V_r}{\partial z} + \frac{\partial V_z}{\partial r} \right), \; e = \frac{\partial V_r}{\partial r} + \frac{V_r}{r} + \frac{\partial V_z}{\partial z}, \tag{6}$$

where $T_{rr}, T_{\theta\theta}, T_{zz}$, and T_{rz} are the components of the stress tensor in the fluid, a_0 is the sound speed in the fluid, and ρ_1 is the perturbation of the fluid density.

Note that Eqs. (3)-(6) are borrowed from the monograph (Guz 2009) and we attempt to impose the appropriate boundary, compatibility and impermeability conditions on the preceding system of equations. Note that in formulating these conditions we have to take into account the following circumstance.

The coordinates r and z in Eqs. (3)-(6) for the compressible viscous fluid flow are the Euler coordinates. However, the coordinates r and z in Eqs. (1) and (2) for the plate motion are the Lagrange coordinates. We recall that in the linear theory of elastodynamics, the difference between the Lagrange and Euler coordinates is not taken into consideration. According to both this fact and the smallness of the perturbation of the quantities related to the fluid, we will ignore the difference between the Euler and Lagrange coordinates, when writing the above conditions.

Thus, we write the boundary conditions on the face plane of the plate. These conditions are

$$Q_{rr}|_{z=0} = -P\delta(r)e^{i\omega t}, \; Q_{rz}|_{z=0} = 0. \tag{7}$$

The compatibility conditions on the plate-fluid interface are

$$Q_{rr}|_{z=-h} = T_{rr}|_{z=-h}, Q_{rz}|_{z=-h} = T_{rz}|_{z=-h}, \left.\frac{\partial u_r}{\partial t}\right|_{z=-h} = V_r|_{z=-h}, \left.\frac{\partial u_z}{\partial t}\right|_{z=-h} = V_z|_{z=-h}. \tag{8}$$

The impermeability conditions on the rigid wall are

$$V_r|_{z=-h-h_d} = 0, V_z|_{z=-h-h_d} = 0. \tag{9}$$

Besides all of these conditions, we must require satisfaction of the following decay conditions

$$\{|Q_{rr}|; |Q_{\theta\theta}|; |Q_{zz}|; |Q_{rz}|; |T_{rr}|; |T_{\theta\theta}|; |T_{zz}|; |T_{rz}|; |u_r|; |u_z|; |V_r|; |V_z|\} \to 0 \text{ as } r \to \infty. \tag{10}$$

3. Method of solution

We consider separately the solution procedures to the field equations related to the plate and fluid.

3.1 Solution procedure to the field equations related to the plate

According to the monograph (Guz 2004), for solutions to Eqs. (1) and (2), we employ the following presentation for the general solution to these equations

$$u_r = -\frac{\partial^2}{\partial r \partial z} X, \quad u_z = \frac{1}{\omega_{1111} + \omega_{1313}} \left(\omega_{1111}\Delta_1 + \omega_{3113} \frac{\partial^2}{\partial z^2} - \rho \frac{\partial^2}{\partial t^2} \right) X \tag{11}$$

where the function X is determined from the equation

$$\left[\left(\Delta_1+(\xi_2)^2\frac{\partial^2}{\partial z^2}\right)\left(\Delta_1+(\xi_3)^2\frac{\partial^2}{\partial z^2}\right)-\rho\left(\frac{\omega_{1111}+\omega_{1331}}{\omega_{1111}\omega_{1331}}\Delta+\frac{\omega_{3333}+\omega_{3113}}{\omega_{1111}\omega_{1331}}\right)\frac{\partial^2}{\partial t^2}+\frac{\rho}{\omega_{1111}\omega_{1331}}\frac{\partial^4}{\partial t^4}\right]X=0,$$
$$\Delta_1=\frac{d^2}{dr^2}+\frac{1}{r}\frac{d}{dr}. \tag{12}$$

The following expressions determine the constants ξ_2 and ξ_3 in (12)

$$(\xi_{2,3})^2=d\pm\left[d^2-\omega_{3333}\omega_{3113}\left(\omega_{1111}\omega_{1331}\right)^{-1}\right]^{\frac{1}{2}},$$
$$d=\left[\omega_{1111}\omega_{3333}+\omega_{1331}\omega_{3113}-(\omega_{1133}+\omega_{1313})^2\right]\times\left(2\omega_{1111}\omega_{1331}\right)^{-1} \tag{13}$$

The notation used in Eqs. (11)-(13) have the expressions given below

$$\omega_{1111}=\lambda+2\mu,\ \omega_{1313}=\mu,\ \omega_{1331}=\mu,\ \omega_{3333}=\lambda+2\mu,\ \omega_{1133}=\lambda,\ \omega_{3113}=\mu. \tag{14}$$

In this way, the solution to Eqs. (1) and (2) is reduced to the solution to Eq. (12). Before considering the solution to Eq. (12), according to the boundary conditions in (7) and the nature of the problem under consideration, we represent all sought quantities as $g(r,z,t)=\bar{g}(r,z)e^{i\omega t}$, where $\bar{g}(r,z)$ is the amplitude of the corresponding quantity. Below we omit the overbar on the amplitude symbols and use the symbol for the amplitude, which is the same as the symbol of the corresponding quantity.

Thus, we obtain the following equation for the X amplitude from Eq. (12) using the above-noted presentation for the sought values

$$\left[\left(\Delta_1+\xi_2^2\frac{\partial^2}{\partial z^2}\right)\left(\Delta_1+\xi_3^2\frac{\partial^2}{\partial z^2}\right)+\frac{\omega^2h^2}{c_2^2}\left(\frac{\lambda/\mu+3}{\lambda/\mu+2}\right)\left(\Delta_1+\frac{\partial^2}{\partial z^2}\right)+\frac{\omega^4h^4}{c_2^4(\lambda/\mu+2)}\right]X=0, \tag{15}$$

where $c_2=\sqrt{\mu/\rho}$.

Note that in writing the Eq. (15), we have used the dimensionless coordinates $\bar{r}=r/h$ and $\bar{z}=z/h$ after the overbars of the dimensionless coordinates have been omitted. Below we also use these dimensionless coordinates. Thus, we attempt to solve the Eq. (26), and for this purpose we employ the Hankel integral representation for the function X

$$X=\int_0^\infty F(k)e^{\chi z}J_0(kr)kdk \tag{16}$$

where $J_0(kr)$ is the Bessel function of the zeroth order.

Substituting (16) into (15), with some mathematical manipulation, we conclude that in order to satisfy Eq. (15), χ must satisfy the algebraic equation

$$A_1\chi^4+B_1\chi^2+C_1=0, \tag{17}$$

where

$$A_1=\xi_2^2\xi_3^2,\ B_1=\frac{\lambda/\mu+3}{\lambda/\mu+2}\frac{(h\omega)^2}{c_2^2}-k^2\left(\xi_2^2+\xi_3^2\right),\quad C_1=-k^2\frac{\lambda/\mu+3}{\lambda/\mu+2}\frac{(h\omega)^2}{c_2^2}+\frac{(h\omega)^4}{c_2^4(\lambda/\mu+2)}+k^4. \tag{18}$$

Consequently, the roots of Eq. (17) we determine as follows

$$\chi_1=\sqrt{-\frac{B_1}{2A_1}+\sqrt{\frac{B_1^2}{4A_1^2}-\frac{C_1}{A_1}}}\,,\ \chi_2=-\chi_1\,,\ \chi_3=\sqrt{-\frac{B_1}{2A_1}-\sqrt{\frac{B_1^2}{4A_1^2}-\frac{C_1}{A_1}}}\,,\ \chi_4=-\chi_3\,. \tag{19}$$

Thus, we determine the following expression for the function X

$$X=\int_0^\infty\left[F_1e^{\chi_1 z}+F_2e^{-\chi_1 z}+F_3e^{\chi_2 z}+F_4e^{-\chi_2 z}\right]J_0(kr)kdk\,. \tag{20}$$

For simplicity of use of the dimensionless coordinates, we change the unknown constants F_n with $h^3\bar{F}_n$, where $(n=1,2,3,4)$ and below we omit the overbar in $\bar{F}_n$. Thus, we determine the following formulae for the displacements by substituting expression (20) into the presentations in (11)

$$\begin{gathered}u_r=h\int_0^\infty\left[F_1\chi_1e^{\chi_1 z}-F_2\chi_1e^{-\chi_1 z}+F_3\chi_2e^{\chi_2 z}\ -F_4\chi_2e^{-\chi_2 z}\right]k^2J_1(kr)dk\,,\\ u_z=h\int_0^\infty\left\{\left[-k^2\frac{\lambda/\mu+2}{\lambda/\mu+1}+\frac{1}{\lambda/\mu+1}\left(\chi_1^2+\frac{(\omega h)^2}{c_2^2}\right)\right]\left(F_1e^{\chi_1 z}+F_2e^{-\chi_1 z}\right)+\right.\\ \left.\left[-k^2\frac{\lambda/\mu+2}{\lambda/\mu+1}+\frac{1}{\lambda/\mu+1}\times\left(\chi_2^2+\frac{(\omega h)^2}{c_2^2}\right)\right]\left(F_3e^{\chi_2 z}+F_4e^{-\chi_2 z}\right)\right\}J_0(kr)kdk\,.\end{gathered} \tag{21}$$

Using the elasticity relations (2) and expressions in (21), we determine the following expressions for the stresses which enter the boundary and compatibility conditions

$$\begin{gathered}Q_{zz}=\mu\int_0^\infty\left\{F_1\left[(\lambda/\mu)k^2\chi_1+(\lambda/\mu+2)\left(-k^2\frac{\lambda/\mu+2}{\lambda/\mu+1}\chi_1\ +\frac{\chi_1}{\lambda/\mu+1}\left(\chi_1^2+\frac{(\omega h)^2}{c_2^2}\right)\right)\right]e^{\chi_1 z}+\right.\\ F_2\left[-(\lambda/\mu)k^2\chi_1+(\lambda/\mu+2)\left(k^2\frac{\lambda/\mu+2}{\lambda/\mu+1}\chi_1\ -\frac{\chi_1}{\lambda/\mu+1}\left(\chi_1^2+\frac{(\omega h)^2}{c_2^2}\right)\right)\right]e^{-\chi_1 z}+\\ F_3\left[(\lambda/\mu)k^2\chi_2+(\lambda/\mu+2)\left(-k^2\frac{\lambda/\mu+2}{\lambda/\mu+1}\chi_2\ +\frac{\chi_2}{\lambda/\mu+1}\left(\chi_2^2+\frac{(\omega h)^2}{c_2^2}\right)\right)\right]e^{\chi_2 z}+\\ \left.F_4\left[-(\lambda/\mu)k^2\chi_2+(\lambda/\mu+2)\left(k^2\frac{\lambda/\mu+2}{\lambda/\mu+1}\chi_2\ -\frac{\chi_2}{\lambda/\mu+1}\left(\chi_2^2+\frac{(\omega h)^2}{c_2^2}\right)\right)\right]e^{-\chi_2 z}\right\}kJ_0(kr)dr\,,\\ Q_{zr}=\mu\int_0^\infty\left\{F_1\left[\chi_1^2-\left(-k^2\frac{\lambda/\mu+2}{\lambda/\mu+1}+\frac{1}{\lambda/\mu+1}\left(\chi_1^2+\frac{(\omega h)^2}{c_2^2}\right)\right)\right]e^{\chi_1 z}+\right.\\ F_2\left[\chi_1^2-\left(-k^2\frac{\lambda/\mu+2}{\lambda/\mu+1}+\frac{1}{\lambda/\mu+1}\left(\chi_1^2+\frac{(\omega h)^2}{c_2^2}\right)\right)\right]e^{-\chi_1 z}+\\ F_3\left[\chi_2^2-\left(-k^2\frac{\lambda/\mu+2}{\lambda/\mu+1}+\frac{1}{\lambda/\mu+1}\left(\chi_2^2+\frac{(\omega h)^2}{c_2^2}\right)\right)\right]e^{\chi_2 z}+\\ \left.F_4\left[\chi_2^2-\left(-k^2\frac{\lambda/\mu+2}{\lambda/\mu+1}+\frac{1}{\lambda/\mu+1}\left(\chi_2^2+\frac{(\omega h)^2}{c_2^2}\right)\right)\right]e^{-\chi_2 z}\right\}k^2J_1(kr)dk\,.\end{gathered} \tag{22}$$

Thus, we determine the expressions of the Hankel integral presentations for the displacements and stresses related to the plate. These expressions contain the unknown constants F_1, F_2, F_3, and F_4, for the determination of which we turn below.

3.2 Solution procedure to the field equations related to the fluid

To solve the field equations related to the fluid flow, we use the following presentations by Guz (Guz 2009) for the general solution to the linearized Navier-Stokes equations

$$V_r = \frac{\partial}{\partial r}\Phi + \frac{\partial^2}{\partial r \partial z}\Psi\,,\; V_z = \frac{\partial}{\partial z}\Phi - \left(\frac{1}{\nu^{(1)}}\frac{\partial}{\partial t} - \frac{\partial^2}{\partial z^2}\right)\Psi\,,$$
$$p_1 = \rho_{01}\left(\frac{\lambda^{(1)}+2\mu^{(1)}}{\rho_{01}}\Delta - \frac{\partial}{\partial t}\right)\Phi\,,\; \rho_1 = \frac{\rho_{01}}{a_0^2}\left(\frac{\lambda^{(1)}+2\mu^{(1)}}{\rho_{01}}\Delta - \frac{\partial}{\partial t}\right)\Phi\,, \tag{23}$$

where the functions Φ and Ψ satisfy the following equations

$$\left[\left(1+\frac{\lambda^{(1)}+2\mu^{(1)}}{a_0^2\rho_{01}}\frac{\partial}{\partial t}\right)\Delta - \frac{1}{a_0^2}\frac{\partial^2}{\partial t^2}\right]\Phi = 0\,,\quad \left(\nu^{(1)}\Delta - \frac{\partial}{\partial t}\right)\Psi = 0\,,\; \Delta = \frac{\partial^2}{\partial r^2} + \frac{1}{r}\frac{\partial}{\partial r} + \frac{\partial^2}{\partial z^2}\,, \tag{24}$$

where $\nu^{(1)}$ is the kinematic viscosity, i.e., $\nu^{(1)} = \mu^{(1)}/\rho_{01}$.

Assuming that $p^{(1)} = -(T_{rr} + T_{\theta\theta} + T_{zz})/3$, we obtain from (6) that $\lambda^{(1)} = -\frac{2}{3}\mu^{(1)}$.

As above, we represent the functions Φ and Ψ as $\Phi(r,z,t) = \bar{\Phi}(r,z)e^{i\omega t}$, and $\Psi(r,z,t) = \bar{\Psi}(r,z)e^{i\omega t}$ respectively, where $\bar{\Phi}(r,z)$ and $\bar{\Psi}(r,z)$ (below we omit the overbar on $\bar{\Phi}(r,z)$ and $\bar{\Psi}(r,z)$) are the amplitude of the corresponding quantity.

For simplicity of use of the dimensionless coordinates we introduce the following presentation for the functions Φ and Ψ

$$\Phi = \omega h^2 \phi\,,\; \Psi = \omega h^3 \psi\,. \tag{25}$$

Thus, we use the Hankel integral presentation $\phi = \int_0^\infty G e^{\delta z} J_0(kr)kdk$ and, substituting this presentation into the first equation in (24) and doing some mathematical calculations, we determine the following expression for the Hankel integral presentation for the function Φ

$$\Phi = \omega h^2 \int_0^\infty \left(G_1 e^{\delta_1 z} + G_2 e^{-\delta_1 z}\right) J_0(kr)kdk\,. \tag{26}$$

where

$$\delta_{1,2} = \pm\sqrt{k^2 - \frac{\Omega_1^2}{1+i\frac{4}{3}\Omega_1^2/N_w^2}}\,,\; \Omega_1 = \frac{\omega h}{a_0}\,,\; N_w^2 = \frac{\omega h^2}{\nu^{(1)}}\,. \tag{27}$$

In a similar manner, we determine the following expression for the function Ψ

$$\Psi = \omega h^3 \int_0^\infty \left(G_3 e^{\gamma_1 z} + G_4 e^{-\gamma_1 z}\right) J_0(kr)kdk\,, \tag{28}$$

where

$$\gamma_{1,2} = \pm\sqrt{k^2 + iN_w^2}\,. \tag{29}$$

Thus, substituting the expressions (26) and (28) into the expressions in (23) and (6), we obtain the following Hankel integral presentations for the velocities and stresses which enter into the boundary and compatibility conditions

$$\begin{aligned}
V_r &= -\omega h\int_0^\infty \left[G_1 e^{\delta_1 z} + G_2 e^{-\delta_1 z} + G_3\gamma_1 e^{\gamma_1 z} - G_4\gamma_1 e^{-\gamma_1 z} \right] k^2 J_1(kr)dk\,,\\
V_z &= \omega h\int_0^\infty \left[G_1\delta_1 e^{\delta_1 z} - G_2\delta_1 e^{-\delta_1 z} + G_3 k^2 e^{\gamma_1 z} + G_4 k^2 e^{-\gamma_1 z} \right] kJ_0(kr)dk\,,\\
T_{zz} &= \mu^{(1)}\omega\int_0^\infty \left\{ \left[-R_0 - \frac{2}{3}\left(\delta_1^2 - k^2\right) + 2\delta_1^2 \right] G_1 e^{\delta_1 z} + \left[-R_0 - \frac{2}{3}\left(\delta_1^2 - k^2\right) + 2\delta_1^2 \right] G_2 e^{-\delta_1 z} + \right.\\
&\left. G_3 2k^2\gamma_1 e^{\gamma_1 z} - G_4 2k^2\gamma_1 e^{-\gamma_1 z} \right\} kJ_0(kr)dk\,,\\
T_{rz} &= \mu^{(1)}\omega\int_0^\infty \left[-2\delta_1 G_1 e^{\delta_1 z} + 2\delta_1 G_1 e^{-\delta_1 z} + \right.\\
&\left. + G_3(-\gamma_1^2 - k^2)e^{\gamma_1 z} + G_4(-\gamma_1^2 - k^2)e^{-\gamma_1 z} \right] k^2 J_1(kr)dr\,,
\end{aligned} \tag{30}$$

where G_1, G_2, G_3, and G_4 are unknown constants and

$$R_0 = -\frac{4}{3}\Omega_1^2\left(1 + i\frac{4\Omega_1^2}{3N_w^2}\right)^{-1} - iN_w^2\,. \tag{31}$$

The above solution procedure can also be easily carried out for the corresponding case of the inviscid fluid, for which we use the representations $V_r = \partial\Phi/\partial r$, $V_z = \partial\Phi/\partial z$, $p_1 = -\rho_{01}\partial\Phi/\partial t$ and $\rho_1 = -\rho_{01}\partial\Phi/(a_0^2\partial t)$, where Φ is determined from the equation $[\Delta - \partial^2/(a_0^2\partial t^2)]\Phi = 0$ and the rheological relationships for the fluid become $T_{zz} = -p_1$ and $T_{rz} = 0$. Using these formulas, the following expressions for the stresses and velocities are obtained: $T_{zz} = \rho_{01} i\omega^2 h^2 \int_0^\infty \left(G_1 e^{\sqrt{k^2-\Omega_1^2}z} + G_2 e^{-\sqrt{k^2-\Omega_1^2}z} \right) J_0(kr)kdk$, $V_r = -\omega h \int_0^\infty \left(G_1 e^{\sqrt{k^2-\Omega_1^2}z} + G_2 e^{-\sqrt{k^2-\Omega_1^2}z} \right) J_1(kr)k^2 dk$, and $V_z = \omega h \int_0^\infty \left(G_1 e^{\sqrt{k^2-\Omega_1^2}z} + G_2 e^{-\sqrt{k^2-\Omega_1^2}z} \right) J_0(kr)kdk$. Moreover, the third compatibility condition in (8) disappears in the case of the inviscid fluid and the second compatibility condition in (8) is replaced by the condition $Q_{rz}|_{z=-h} = 0$. In addition, the first impermeability condition in (9) also disappears in the case of the inviscid fluid.

3.3 Obtaining the equations for the determination of the unknown constants

The unknown constants F_1, F_2 ,F_3 , and F_4 which enter into the expressions of the stresses and displacements of the plate, and the unknown constants G_1, G_2, G_3, and G_4, which enter into the expressions of the velocities and stresses of the fluid, are determined from the boundary (7), compatibility (8), and impermeability (9) conditions. Under obtaining the algebraic equations

containing these unknowns, it is necessary to obtain the Hankel transform of the function $P\delta(r)$ which is on the left side in the first boundary condition in (7). For this purpose, we present the function $P\delta(r)$ as $\lim_{r\to 0}\frac{P_0}{(h^2\pi r^2)}$ (here r is a dimensionless coordinate and P_0 has the force dimension, however, P has the stress dimension, i.e., P is presented as P_0/h^2). From $\lim_{\varepsilon\to 0}\int_0^{\varepsilon}\frac{P_0 J_0(kr)rdr}{h^2\pi\varepsilon^2}$ we obtain $\frac{P_0}{h^2 2\pi}$ for the Hankel transform of $P\delta(r)$. After this preparation, we obtain the following equations concerning the above unknown constants

$$
\begin{gathered}
Q_{zz}\big|_{z=0}=-P\delta(r)\Rightarrow\sum_{n=1}^{4}a_{1n}F_n=-\frac{P_0}{h^2 2\pi},\qquad Q_{zr}\big|_{z=0}=0\Rightarrow\sum_{n=1}^{4}a_{2n}F_n=0,\ Q_{zz}\big|_{z=-h}-T_{zz}\big|_{z=-h}=0\Rightarrow\\
\sum_{n=1}^{4}a_{3n}F_n-M\sum_{n=1}^{4}b_{3n}G_n=0,\\
Q_{zr}\big|_{z=-h}-T_{zr}\big|_{z=-h}=0\Rightarrow\ \sum_{n=1}^{4}a_{4n}F_n-M\sum_{n=1}^{4}b_{4n}G_n=0,\\
\left.\frac{\partial u_r}{\partial t}\right|_{z=-h}-V_r\big|_{z=-h}=0\Rightarrow\ \sum_{n=1}^{4}a_{5n}F_n-\sum_{n=1}^{4}b_{5n}G_n=0,\\
\left.\frac{\partial u_r}{\partial t}\right|_{z=-h}-V_r\big|_{z=-h}=0\Rightarrow\ \sum_{n=1}^{4}a_{5n}F_n-\sum_{n=1}^{4}b_{5n}G_n=0,\\
\left.\frac{\partial u_z}{\partial t}\right|_{z=-h}-V_z\big|_{z=-h}=0\Rightarrow\ \sum_{n=1}^{4}a_{6n}F_n-\sum_{n=1}^{4}b_{6n}G_n=0,\\
V_r\big|_{z=-h-h_d}=0\Rightarrow\sum_{n=1}^{4}b_{7n}G_n=0,\ V_z\big|_{z=-h-h_d}=0\Rightarrow\sum_{n=1}^{4}b_{8n}G_n=0,
\end{gathered}
\tag{32}
$$

where $M=\mu^{(1)}\omega/\mu$.

Note that the explicit expressions of the coefficients a_{jn} and b_{mn} $(n=1,2,3,4)$, $(j=1,2,\ldots,6)$, $(m=3,4,\ldots,8)$ can easily be determined from the expressions in (21), (22), and (30). Therefore, these expressions are not given here.

After determining the unknown constants above, we determine the Hankel integral presentations of all the sought quantities. Determination of the amounts sought from these presentations is made numerically by the algorithm, which we discuss in the next section.

4. Numerical results and discussions

First, we consider some remarks on the calculation algorithm of the integrals in the Hankel integral presentation of the sought quantities. Then, we analyze the numerical results related to the frequency response of the normal stress acting on the interface plane between fluid and plate.

4.1 On the calculation algorithm of the integrals in (21), (22), and (30)

We can present the unknowns F_1, F_2, F_3, F_4, G_1, G_2, G_3, and G_4 in (32) via the formulae

$$
Z_q=\frac{\det\left\|\beta_{nm}^{q}\right\|}{\det\left\|a_{nm}\right\|},\ n;m=1,2,...,8,\ q=1,2,...,8,\ Z_j=F_j,\ Z_{j+4}=G_j,\ j=1,2,3,4,
\tag{33}
$$

where the matrix (β_{nm}^{q}) is obtained from the matrix (a_{nm}) by replacing the $q-th$ column of the latter with the column $(-P_0/(2\pi h^2),0,0,0,0,0,0,0)^T$.

According to this statement, if we take the Hankel integral transform parameter k as the wavenumber, the equation

$$\det\|a_{nm}\| = 0 \tag{34}$$

coincides with the dispersion equation of the axisymmetric waves with the velocity ω/k propagating in the radial direction. It should be noted that, according to the well-known physico-mechanical consideration, the Eq. (34) must have complex roots only for the system being considered. This character of the roots is caused by the viscosity of the fluid. However, as usual, the viscosity of the Newtonian fluids is insignificant in the quantitative sense. Therefore, in some cases within the scope of the PC calculation accuracy, the Eq. (34) may have "real roots". Moreover, in the cases where the fluid is modeled as an inviscid fluid, the Eq. (34) has real roots. In such cases, according to the expressions in (33), these roots become singular points of the integrated expressions in (21), (22), and (30).

The algorithm for the calculation of the wavenumber integrals in such cases is discussed in the monograph (Akbarov 2015) and in many references listed therein, according to which, in indicated cases, the wavenumber integrals in (21), (22), and (30) may be evaluated along the Sommerfeld contour. According to this algorithm, the integration concerning $k \in [0,\infty]$ is transformed into the integration concerning $(k_1 + i\varepsilon) \in [0 + i\varepsilon, \infty + i\varepsilon]$, where ε is constant and $\varepsilon << 1$, and e is selected according to the convergence and smoothness of the obtained numerical results. In this way, the singular points of the integrated functions in (21), (22), and (30) are avoided. However, this "avoidance" takes place only in cases where the order of the singularity is less than 1. In cases where the order of the singularity is greater than one, the Sommerfeld contour method cannot avoid the case relating to the resonance phenomenon.

In the present investigations, the Sommerfeld contour method is employed only in the case where the fluid is modeled as an inviscid one, and the value of ε is determined as $\varepsilon = 0.0001$. However, in the cases where the fluid is modeled as viscous, the wavenumber integrals are calculated directly without employing the Sommerfeld contour method.

Moreover, under calculation procedures, the improper integrals $\int_0^{\infty}(\bullet)dk$ in (21), (22), and (30) are replaced by the corresponding definite integrals $\int_0^{S_1^*}(\bullet)dk$. The values of S_1^* are determined from the convergence requirement of the numerical results. Note that under calculation of the latter integrals, the integration intervals are further divided into a certain N number of shorter intervals, which are used in the Gauss integration algorithm. The values of the integrated expressions at the sample points are calculated through the equations in (32). All these procedures are performed automatically with the PC programs constructed by the authors in MATLAB.

Consequently, numerical results which will be considered below are calculated by the following expressions

$$T_{zz} = \mu^{(1)}\omega \operatorname{Re}\left\langle e^{i\omega t}\int_0^{S_1^*}\left\{\left[-R_0 - \frac{2}{3}\left(\delta_1^2 - k^2\right) + 2\delta_1^2\right]G_1 e^{\delta_1 z} + \left[-R_0 - \frac{2}{3}\left(\delta_1^2 - k^2\right) + 2\delta_1^2\right]G_2 e^{-\delta_1 z} + G_3 2k^2\gamma_1 e^{\gamma_1 z} - G_4 2k^2\gamma_1 e^{-\gamma_1 z}\right\} kJ_0(kr)dk\right\rangle. \tag{35}$$

This completes the discussions related to the algorithms employed for calculation of the

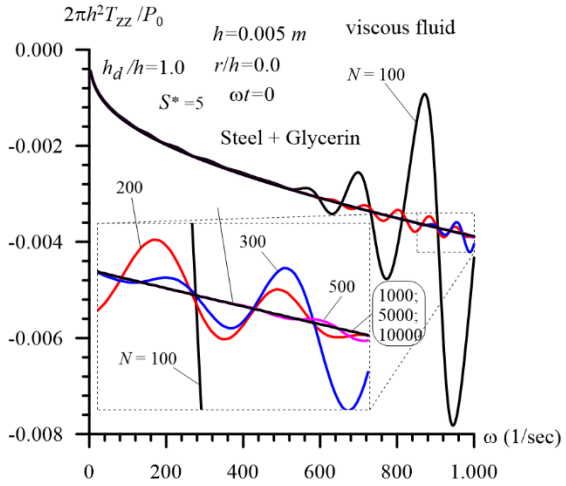

Fig. 2 Convergence of the numerical results related to the stress $2\pi h^2 T_{zz}/P_0$ with respect to the number N in the case where $S_1^* = 5$

wavenumber integrals in (21), (22), and (30).

4.2 Testing the convergence of the used algorithm

In the numerical results, which are discussed below, the values of S_1^* are determined, (as noted above) from the convergence criterion of the calculated integrals in (21), (22), and (30). For illustration of this convergence, we consider the case where $h = 0.005\,\text{m}, 4(1/\text{sec}) \le \omega \le 1000(1/\text{sec})$, and $h_d/h = 1.0$. As noted above, under calculation of the related integrals, the interval $0 \le k \le S_1^*$ is divided into a certain number of shorter intervals. Let us denote this number through N. Consequently, the length of the shorter intervals is S_1^*/N and in each of these shorter intervals, the integration is made by the use of the Gauss integration algorithm with ten sample points. Consequently, the convergence of the numerical integration can be estimated with respect to the values of S_1^* and N.

In the numerical investigation, we assume that (if not otherwise specified) the material of the plate-layer is Steel with mechanical constants $\mu = 79 \times 10^9$ Pa and $\lambda = 94.4 \times 10^9$ Pa, and density $\rho = 7790\ \text{kg/m}^3$ (Guz 2004), and the material of the fluid is Glycerin with a viscosity coefficient $\mu^{(1)} = 1.393\ \text{kg/(m} \times \text{sec)}$, density $\rho = 1260\ \text{kg/m}^3$ and sound speed $a_0 = 1927\ \text{m/sec}$ (Guz 2009). We also introduce the notation $c_2 = \sqrt{\mu/\rho}$ which is the shear wave propagation velocity in the plate material.

Note that for the chosen fluid and for the considered range of change in the frequency of the external force, the ratio $4\Omega_1^2/(3N_w^2)$ has the order of magnitude 10^{-6}, according to which it can be neglected with respect to the 1 in expressions (27)-(31).

Thus, we consider examples on the convergence of the numerical results with respect to the aforementioned number N in the case where $S_1^* = 5$. The graphs given in Fig. 2 illustrate the frequency response of the dimensionless stress $2\pi h^2 T_{zz}/P_0$ (Fig. 2) under $\omega t = 0$ and $r/h = 0$. Note that under construction of these graphs (as well as all graphs illustrated below), the values of the velocities and stresses are calculated on the interface plane (i.e., at $z = -h$) between the fluid

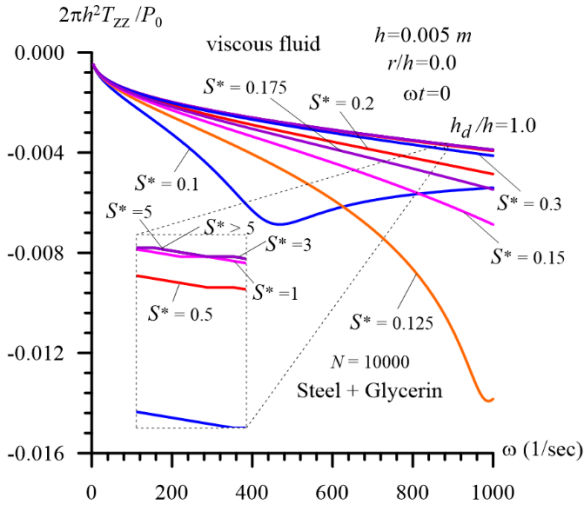

Fig. 3 Convergence of the numerical results related to the stress $2\pi h^2 T_{zz}/P_0$ with respect to the S_1^*in the case where $N = 10000$

and the plate. It follows from Fig. 2 that the values of the velocity and stress approach a certain asymptote with the number$N$.

In other words, the numerical results obtained for the studied quantities approach a certain limit with the number N and after a certain value of N (denote it by N^*), the numerical results obtained for the various $N > N^*$ coincide with each other with accuracy 10^{-6}. It should be noted that the value of N^* depends not only on the frequency ω, but also on the other problem parameters and mainly on h and h_d/h. For instance, for the case under consideration it can be taken that $N^* = 1000$. Nevertheless, to guarantee accuracy in the convergence sense with respect to the number N, all the numerical results presented and discussed in the present paper are obtained in the case where $N = 10000$.

The results illustrated in Fig. 3 show the convergence of the numerical results with respect to the values of S_1^* in the case where $N = 10000$. These results are presented for the dimensionless stress $2\pi h^2 T_{22}/P_0$ which are also obtained in the case where $h = 0.005\ \text{m}, 4(1/\text{sec}) \leq \omega \leq 1000(1/\text{sec})$, and $h_d/h = 1.0$. It follows from these results that the value $S_1^* = 5$ is more than enough to obtain convergence of the numerical results with accuracy 10^{-6}. Therefore, all the numerical results presented below are obtained in the case where $S_1^* = 5$.

The results above can also be taken as the reliability of the analytical solution method and the numerical results. Moreover, the reliability of the numerical results will be confirmed by the agreement of the results with the known physico-mechanical considerations related to the studied phenomenon, as discussed below. Unfortunately, we have not found in the literature any corresponding numerical results to compare with the present ones.

4.3 The influence of fluid viscosity on the frequency response of the stress

In this subsection, we consider and analyze the numerical results illustrating the influence of the fluid viscosity on the frequency response of the interface normal stress. Thus, consider the graphs in Figs. 4, 5, and 6 which are the frequency response of the dimensionless stress

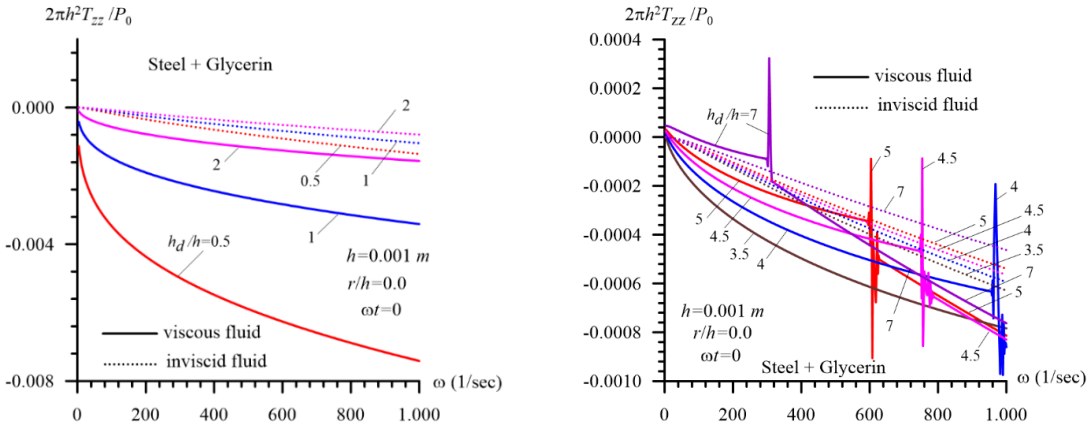

(a) $h_d/h = 0.5, 1.0, 2.0$ (b) $h_d/h = 3.5, 4.0, 4.5, 5.0, 7.0$

Fig. 4 Frequency response of the dimensionless stress $2\pi h^2 T_{zz}/P_0$ in the case where $h = 0.001$ m

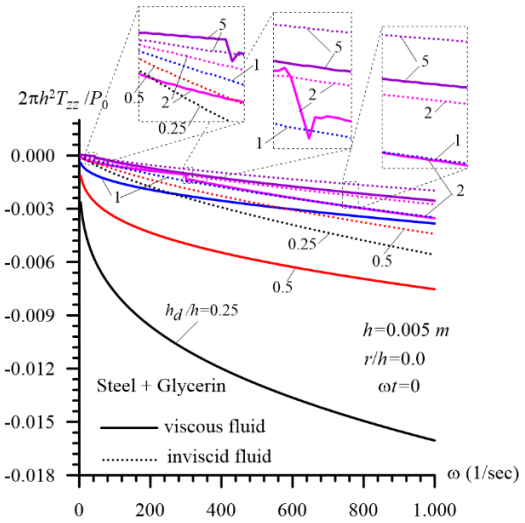

Fig. 5 Frequency response of the dimensionless stress $2\pi h^2 T_{zz}/P_0$ in the case where $h = 0.005$ m under various h_d/h

$2\pi h^2 T_{zz}/P_0$ constructed in the cases where $h = 0.001$ m, 0.005 m, and 0.01 m, respectively under various values of the ratio h_d/h at $\omega t = 0$ and $r/h = 0$. Note that in these figures, the graphs drawn with the dashed lines relate to the inviscid fluid case. Consequently, comparing these graphs with the corresponding graphs drawn with solid lines shows the influence of the fluid viscosity on the frequency response of the quantities under consideration. Moreover, note that in the inviscid fluid case maximum value of the dimensionless stress $2\pi h^2 T_{zz}/P_0$ with respect to ωt appears at $\omega t = 0$.

Thus, we analyze the graphs given in Fig. 4, according to which, under $h = 0.001$ m in the considered change range of the frequency ω under $h_d/h \leq 3.5$, the absolute values of the dimensionless stress $2\pi h^2 T_{zz}/P_0$ increase monotonically with the frequency, and the fluid viscosity causes these values to increase significantly, concerning the corresponding ones obtained

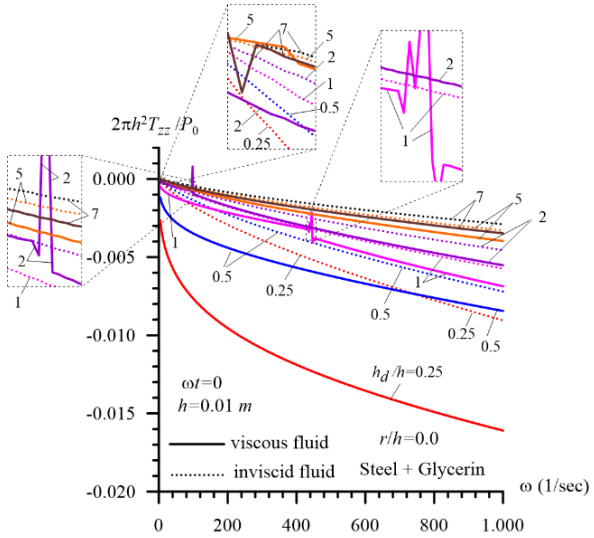

Fig. 6 Frequency response of the dimensionless stress $2\pi h^2 T_{zz}/P_0$ in the case where $h = 0.01$ m under various h_d/h

for the inviscid fluid case. At the same time, these results show that under $h_d/h \leq 3.5$, an increase in the values of the ratio h_d/h (i.e., an increase in the fluid depth) causes the absolute values of the stress to decrease.

However, under $h_d/h \geq 4$, "zigzag" places appear resembling a resonant phenomenon in the stress and velocity frequency responses. The values of the frequency ω (denoted by $\omega*$) in the near vicinity of which (i.e., in $\omega \in (\omega* - \delta_1, \omega* + \delta_1)$) the above "zigzag" places appear, decrease with h_d/h. This phenomenon is observed not only in Fig. 4(b) and Fig. 7, related to the case where $h = 0.001$ m, but also in Figs. 5 and 6 related to the cases where $h = 0.005$ m and $h = 0.01$ m, respectively. It follows from the comparison of the results presented in Figs. 4, 5, and 6 with each other that the value of h_d/h, after which the above "zigzag" places appear, decreases with the plate thickness. The results also show that the appearance of the "zigzag" places relates only to the viscous fluid case. In other words, such areas do not appear in the frequency responses obtained in the inviscid fluid case. This allows us to conclude that in the system under consideration, the appearance of the "zigzag" places on the frequency responses is caused by the fluid viscosity.

At the same time, analyses of the results allow us to say that the character of the frequency responses before and after the "zigzag" places $\omega \in (\omega* - \delta_1, \omega* + \delta_1)$ differ from each other. Consequently, it seems the existence of the "zigzag" places leads to translation of the frequency response mode to another mode. As a result, the character of the influence of the fluid viscosity on the values of the stress changes. As usual, as follows from Figs. 4, 5, and 6, after the "zigzag" place, the absolute values of the stress increase more rapidly with frequency.

Note that the "zigzag" phenomenon on the frequency responses is not observed in the paper (Akbarov and Ismailov 2017) which studied the corresponding problem for the plane-strain state. However, the results on the influence of the fluid viscosity on the absolute values of the stress and velocity agree in the qualitative sense with the corresponding ones obtained in the paper (Akbarov and Ismailov 2017).

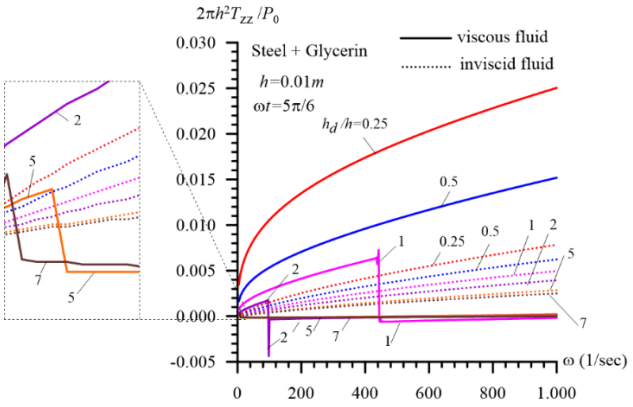

Fig. 7 Frequency response of the dimensionless stress $2\pi h^2 T_{zz}/P_0$ in the case where $\omega t = 5\pi/6$ under $h = 0.01$ m for various h_d/h

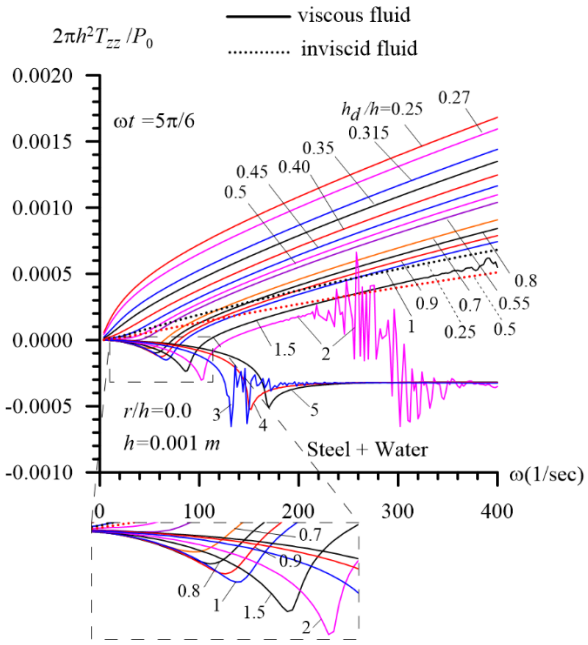

Fig. 8 Frequency response of the dimensionless stress $2\pi h^2 T_{zz}/P_0$ in the case where the plate material is Steel, and water is selected as the fluid, under $\omega t = 5\pi/6$ and $h = 0.001$ m for various h_d/h

Moreover, note that, according to the above results, the appearance of the "zigzag" place and the magnitude of $\omega *$ depend on the plate thickness and the ratio h_d/h. However, as can be predicted, the appearance of the "zigzag" place and the magnitude of $\omega *$ do not depend on the vibration phase ωt for the selected pairs of materials for the plate and fluid. As an example of the non-dependence of the appearance of the "zigzag" place and the value of $\omega *$ on ωt, we consider the frequency responses presented in Fig. 7 which are constructed in the case where $\omega t = 5\pi/6$ for the dimensionless stress $2\pi h^2 T_{zz}/P_0$, under $h = 0.01$ m for the various values of h_d/h.

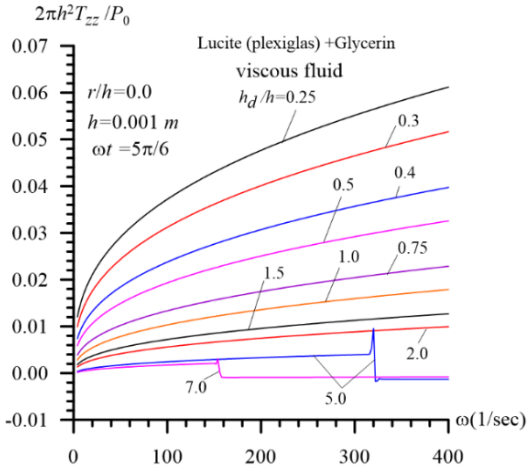

Fig. 9 Frequency response of the dimensionless stress $2\pi h^2 T_{zz}/P_0$ in the case where the plate material is Lucite, and Glycerin is selected as the fluid, under $\omega t = 5\pi/6$ and $h = 0.001$ m for various h_d/h

Comparison of the graphs in Fig. 7 with the graphs in Fig. 6 confirms the above conclusion on the non-dependence of the appearance of the "zigzag" place and the non-dependence of the values of $\omega*$ on the vibration phase ωt.

Furthermore, the values of $\omega*$ and the values of h_d/h, after which the above "zigzag" place on the frequency response appears, and the behavior of the frequency response in this place depend on the material properties of the fluid and the plate. To confirm this statement, we consider the graphs illustrated in Fig. 8, (Fig. 9) which show the frequency response of the dimensionless stress $2\pi h^2 T_{zz}/P_0$ in the case where the plate material, as in the cases above, is Steel, however, water is selected as the fluid (the plate material is Lucite, however, Glycerin is selected as the fluid). The graphs of these figures are constructed for the case where $h = 0.001$ m and $\omega t = 5\pi/6$ under various values of the ratio h_d/h. Under calculation procedure, the mechanical properties for the water are selected as $\mu^{(1)} = 1.3 \times 10^{-3}$ kg/(m × sec) (viscosity coefficient), $\rho = 1000$ kg/m^3 (density) and $a_0 = 1459.4$ m/sec (sound speed) (Guz 2009); however, the mechanical properties for Lucite as $\mu = 1.86 \times 10^9$ Pa, $\lambda = 3.96 \times 10^9$ Pa and $\rho = 1160$ kg/m^3 (density) (Guz 2004).

Under construction of these graphs, for clarity, we assume that $4(1/sec) \leq \omega \leq 400(1/sec)$. To accurately identify the impact of h_d/h on the frequency response in Fig. 8, the corresponding graphs are constructed for many subsequent values of h_d/h, each of which is distinguished from the previous one with a small step.

Thus, it follows from Fig. 8 that in the "Steel+water" case, after a certain value of the ratio h_d/h, the frequency responses have a non-monotonic character, and there exists a frequency (denoted by ω') at which $d(2\pi h^2 T_{zz}/P_0)/d\omega = 0$, and the values of ω' increase with h_d/h. At the same time, it follows from the results in Fig. 8 that the "zigzag" places also appear in the frequency responses. Consequently, the fluid properties can change the character of the frequency responses. However, these properties cannot cause the disappearance of the "zigzag" places.

Analyses of the graphs in Fig. 9 show that in the "Lucite+Glycerin" case, the change in the plate material properties concerning the "steel+ glycerin" case causes only quantitative change in the frequency responses.

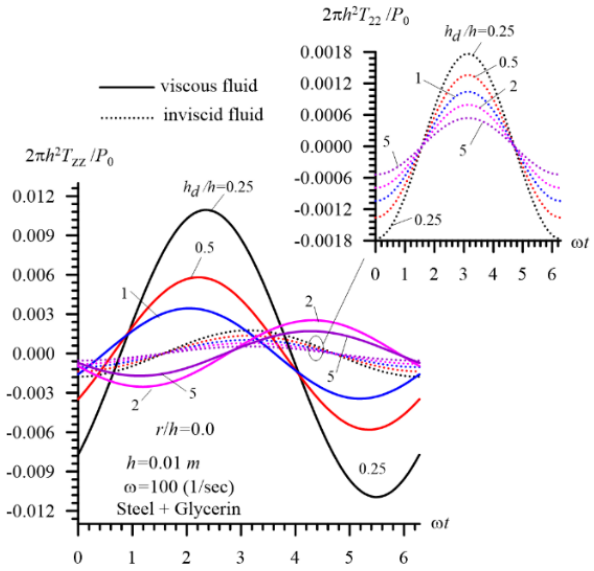

Fig. 10 Change of the dimensionless stress $2\pi h^2 T_{zz}/P_0$ with respect to the vibration phase ωt under $\omega = 100(1/\sec)$ in the cases where $h = 0.01$ m

Thus, we complete the consideration of the numerical results related to the frequency response of the interface stress, and of the analyses of the influence of the problem parameters such as fluid viscosity, fluid depth, and plate thickness on this response. However, in all these considerations, we have assumed that the vibration phase $\omega t$is fixed and $\omega t = 0$ or $\omega t = 5\pi/6$. Now we consider the numerical results illustrating the influence of the vibration phase on the values of the stress under consideration. Before considering these results, we recall the following statement.

According to the expressions (6), (23), and (24), in the inviscid fluid case, we obtain the presentations $T_{rr} = T_{\theta\theta} = T_{zz} = -p_1$, $p_1 = -\rho_{01}\partial\Phi/\partial t$, $V_r = -\partial\Phi/\partial r$, and $V_z = \partial\Phi/\partial z$. In the case where we select the function Φ as $\bar{\Phi}\ (r,z)\,sin(\omega t)$, the stresses T_{rr}, $T_{\theta\theta}$, and T_{zz} change with respect to time as $cos(\omega t)$. Consequently, in the inviscid fluid case, the values of the vibration phase, at which the stresses have their absolute maximum, are $\omega t = 0 + n\pi$, and $n = 0,1,2,\ldots$. However, this rule is violated in the viscous fluid case, and it is impossible to say a priori at what vibration phases the stresses have their absolute maximum. These vibration phases can be determined from the numerical results showing the dependencies of the quantities on the vibration phase.

For this purpose, we consider the graphs of the dependence between the dimensionless stress $2\pi h^2 T_{zz}/P_0$ and ωt (where $0 \le \omega t \le 2\pi$). The results are presented in Fig. 10 for the cases where $h = 0.01$ m. Note that these results are obtained in the case where $\omega = 100(1/\sec)$, and in this figure the corresponding results related to the inviscid fluid case are also given.

Thus, from the analyses of the results in Fig. 10, the values of ωt, denoted by $(\omega t)*$ and $(\omega t)**$, at which the stress has its absolute maximum are in $(0,\pi)$ and in $(\pi,2\pi)$, i.e., $(\omega t)*\in (0,\pi)$, $(\omega t)**\in(\pi,2\pi)$, and $(\omega t)**=(\omega t)*+\pi$. Moreover, the results show that $(\omega t)*$ and $(\omega t)**$decrease with h_d/h. However, the sign change takes place in the absolute values of the stress appearing under relatively small values of the ratio h_d/h. This situation can be explained with the nearest frequency $\omega = 100(1/\sec)$ to the corresponding "zigzag" place discussed above

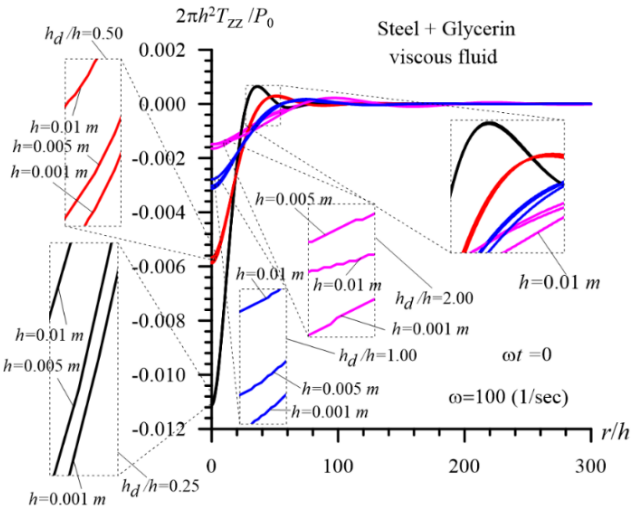

Fig. 11 Distribution of the stress $2\pi h^2 T_{zz}/P_0$, with respect to r/h under $\omega t = 0$ and $\omega = 100(1/\sec)$ for various h_d/d and h

and appearing in the relatively great values of h_d/h (see Figs. 5 and 6).

All the above results are calculated at point $r/h = 0$ on the interface plane. Now we consider the results illustrating the distribution of the stress and velocities concerning r/h. The results related to these distributions are given in Fig. 11 for the stress $2\pi h^2 T_{zz}/P_0$. These results are obtained under $\omega t = 0$ and $\omega = 100(1/\sec)$ for various h_d/h and h, the values of which are indicated in the figures.

These results show the decaying rule of the stress with r/h and that the stress $2\pi h^2 T_{zz}/P_0$ have their absolute maximum value at point $r/h = 0.0$. From Fig. 11, it follows that a decrease in the values of h, in general, leads to a decrease in the absolute values of the stress.

The present paper investigates the axisymmetric forced vibration of the hydro-elastic system consisting of the elastic plate, compressible viscous fluid, and rigid wall. The motion of the plate is described by the exact equations and relations of linear elastodynamics, however, the flow of the compressible viscous fluid is described by the linearized Navier-Stokes equations. The corresponding boundary-contact problem is solved by employing the Hankel integral transform. Originals of the sought values are found numerically by using the algorithms and PC programs developed by the authors. Numerical results on the frequency response are presented and discussed for the normal stress on the interface plane between the fluid and plate. It is found that the fluid viscosity increases the absolute values of the stress.

The main difference between the present results and the corresponding results obtained in the plane-strain case studied in the paper (Akbarov and Ismailov 2017) can be formulated as follows:

- in the axisymmetric case, with specific values of the problem parameters, “zigzag” places, (resembling the resonance phenomenon), appear on the frequency responses. However, such a phenomenon was not observed in the paper (Akbarov and Ismailov 2017);
- the appearance of the “zigzag” places is observed only in the viscous fluid case; in the inviscid fluid cases, as in the plane strain case (Akbarov and Ismailov 2017), they are not observed;
-it follows from the two conclusions above that the fluid viscosity leads to the appearance of

"zigzag" places in the axisymmetric case;

In our opinion, as outlined above, the qualitative difference between the results of the axisymmetric and plane-strain cases is caused by the difference in the character of the nature of the studied phenomenon, namely, in the reflection characteristics of the waves in the axisymmetric and plane-strain cases.

Finally, note that the results obtained in the present paper can be used for qualitative estimation in the prognosis and controlling of the energy harvesting systems detailed in the paper (Kang *et al*. 2024).

References

Abdelbaki, B.M., Sayed Ahmed, M.E. and Al Kaisy, A.M. (2022), "A parametric study on the free vibration of a functionally graded material circular plate with non-uniform thickness resting on a variable Pasternak foundation by differential quadrature method", *Couple. Syst. Mech.*, **11**(4), 357-371. https://doi.org/10.12989/csm.2022.11.4.357

Akbarov, S.D. (2015), *Dynamics of Pre-strained Bi-material Elastic Systems: Linearized Three-Dimensional Approach*, Springer, Heidelberg, New York, USA.

Akbarov, S.D. (2018), "Forced vibration of the hydro-viscoelastic and-elastic systems consisting of the viscoelastic or elastic plate, compressible viscous fluid, and rigid wall: A review", *Appl. Comput. Math.*, **17**(3), 221-245.

Akbarov, S.D. and Bagirov, E.T. (2022), "The dispersion of the axisymmetric wave propagating in the pre-strained highly elastic plate under bi-lateral contact with a fluid", *Wave. Random Complex Media*, 1-37. https://doi.org/10.1080/17455030.2022.2147246.

Akbarov, S.D. and Bagirov, E.T. (2023), "Dispersion of the axisymmetric waves propagating in the hydro-elastic system consisting of the pre-strained highly elastic plate, compressible inviscid fluid, and rigid wall", *Arch. Appl. Mech*., **93**, 861-879. https://doi.org/10.1007/s00419-022-02304-0.

Akbarov, S.D. and Huseynova, T. (2019), "Forced vibration of the hydro-elastic system consisting of the orthotropic plate, compressible viscous fluid, and rigid wall", *Couple. Syst. Mech.*, **8**(3), 199-218. https://doi.org/10.12989/csm.2019.8.3.199.

Akbarov, S.D. and Ismailov, M.I. (2016), "Frequency response of a pre-stressed metal elastic plate under compressible viscous fluid loading", *Appl. Comput. Math*., **15**(2), 172-188.

Akbarov, S.D. and Ismailov, M.I. (2017), "The forced vibration of the system consisting of an elastic plate, compressible viscous fluid, and rigid wall", *J. Vib. Control*, **23**(11), 1809-1827. https://doi.org/10.1177/1077546315601299.

Akbarov, S.D. and Ismailov, M.I. (2018), "The influence of the rheological parameters of a hydro-elastic system consisting of a viscoelastic plate, viscous fluid, and rigid wall on the frequency response of this system", *J. Vib. Control*, **24**(7), 1341-1363. https://doi.org/10.1177/1077546316660029.

Akbarov, S.D. and Negin, M. (2021), "On the dispersion of waves propagating in "plate+fluid layer", systems", *Couple. Syst. Mech.*, **10**(2), 123-142. https://doi.org/10.12989/csm.2021.10.2.123.

Akbarov, S.D. and Negin, M. (2023), "Attenuation of quasi-Lamb waves in a hydroelastic system "elastic plate+compressible viscous fluid+rigid wall", *Struct. Eng. Mech.*, **81**(4), 443-459. https://doi.org/10.12989/sem.2022.81.4.443.

Askari, E., Jeong, K.H., Ahn, K.H. and Amabili, M. (2020), "A mathematical approach to study fluid-coupled vibration of eccentric annular plates", *J. Fluid. Struct.*, **98**, 103129. https://doi.org/10.1016/j.jfluidstructs.2020.103129

Bagno, A.M. (2017a), "Dispersion properties of Lamb waves in an elastic layer-ideal liquid half-space system", *Int. Appl. Mech.*, **53**(6), 609-616. https://doi.org/10.1007/s10778-018-0843-9.

Bagno, A.M. (2017b), "Effect of prestresses on the dispersion of quasi-Lamb waves in the system consisting

of an ideal liquid layer and a compressible elastic layer", *Int. Appl. Mech.*, **53**(2), 139-148. https://doi.org/10.1007/s10778-017-0799-1.

Cao, Y., Carrera, E., Rudykh, S. and Chen, W. (2024), "Axisymmetric vibration of multilayered electroactive circular plates in contact with fluid", *J. Sound Vib.*, **573**, 118189, https://doi.org./j.jsv.2023.118189.

Ekicioglu Kuzeci, E. and Akbarov, S.D. (2023a), "The influence of the coupling effect of physical-mechanical fields on the forced vibration of the hydro-piezoelectric system consisting of a PZT layer and a viscous fluid with finite depth", *Struct. Eng. Mech.*, **85**(2), 247-263. https://doi.org/10.12989/sem.2023.85.2.247.

Ekicioglu Kuzeci, E. and Akbarov, S.D. (2023b), "Vibration of a two-layer "metal+pzt" plate contacting with viscous fluid", *Comput. Mater. Continua*, **74**(2), 4337-4361. https://doi.org/10.32604/cmc.2023.033446.

Guz, A.N. (2004), *Elastic Waves in Bodies with Initial (Residual) Stresses*, A.C.K. Kiev, Ukraine. (in Russian)

Guz, A.N. (2009), *Dynamics of Compressible Viscous Fluid*, Cambridge Scientific Publishers, England.

Guz, A.N. and Bagno, A.M. (2017), "Effect of liquid viscosity on dispersion of quasi-Lamb waves in an elastic-layer-viscous-liquid-layer system", *Int. Appl. Mech.*, **53**(4), 361-367. https://doi.org/10.1007/s10778-017-0819-1.

Guz, A.N. and Bagno, A.M. (2018), "Effect of prestresses on the dispersion of lamb waves in a system consisting of a viscous liquid layer and a compressible elastic layer", *Int. Appl. Mech.*, **54**(3), 249-258. https://doi.org/10.1007/s10778-018-0902-2.

Guz, A.N. and Bagno, A.M. (2019), "Propagation of quasi-lamb waves in an elastic layer interacting with a viscous liquid half-space", *Int. Appl. Mech.*, **55**(5), 459-469. https://doi.org/10.1007/s10778-019-00968-w.

Hadj, B., Rabia, B. and Daouadji, T.H., (2021), "Vibration analysis of porous FGM plate resting on elastic foundations: Effect of the distribution shape of porosity", *Couple. Syst. Mech.*, **10**(1), 61-77. https://doi.org/10.12989/csm.2021.10.1.061.

Iurlov, M.A., Kamenskikh, A.O., Lekomtsev, S.V. and Matveenko, V.P. (2022), "Passive suppression of resonance vibrations of a plate and parallel plates assembly, interacting with a fluid", *Int. J. Struct. Stab. Dyn.*, **22**(09), 2250101. https://doi.org/10.1142/S0219455422501012

Kang, X., Huang, Q., Wu, Z., Tang, J. and Jiang, X. (2024), "A review of the tuned mass damper inerter (TMDI) in energy harvesting and vibration control: designs, analysis and applications", *CMES-Comput. Model. Eng. Sci.*, **139**(3), 2361-2398. https://doi.org/10.32604/cmes.2023.043936.

Koçal, T. (2020), "The dynamical behavior of the moving viscoelastic plate in contact with viscous fluid with finite depth under action of time-harmonic forces", *Ocean Eng.*, **215**, 107840. https://doi.org/10.1016/j.oceaneng.2020.107840.

Lamb, H. (1921), "Axisymmetric vibration of circular plates in contact with water", *Proc. R Soc., London, UK*, 205-216.

Paimushin, N.V. and Gazizullin, R.K. (2021), "Free and forced vibrations of a composite plate in a perfect compressible fluid, taking into account energy dissipation in the plate and fluid", *Lobachevskii J. Math.*, **42**(8), 2016-2022.

Paimushin, V.N., Tarlakovskii, D.V., Firsov, V.A. and Gazizullin, R.K. (2020), "Free and forced bending vibrations of a thin plate in a perfect compressible fluid with energy dissipation taken into account", *ZAMM-J. Appl. Math. Mech./Zeitschrift für Angewandte Mathematik und Mechanik*, **100**(3), e201900102. https://doi.org/10.1002/zamm.201900102.

Popov, V.S., Mogilevich, L.I. and Popova, A.A. (2024), "Nonlinear oscillations of a plate resting on a nonlinear elastic foundation and forming the bottom of a plane channel filled with a viscous gas", *Russ. J. Nonlin. Dyn.*, **20**(4), 581-599. https://doi.org/10.20537/nd241101.

Taati, E., Rastian, V. and Fallah, F. (2024), "Nonlinear geometric fluid-structure interaction model of multilayered sandwich plates in contact with unbounded or bounded fluid flow", *Ocean Eng.*, **292**, 116559. https://doi.org./10.1016/j.oceaneng.2024.116559.

Ulbricht, N., Boldini, A., Zhang, P. and Porfiri, M. (2024), "Three-dimensional analytical solution of free

vibrations of a simply supported composite plate in contact with a fluid", *J. Sound Vib.*, **572**, 118139. https://doi.org/10.1016/j.jsv.2023.118139.

Wu, Q.Y., Khabakhpasheva, T.I., Ni, B.Y. and Korobkin, A.A. (2023), "Small-amplitude waves in a floating poroelastic plate forcing by vertical pitching plate", *Phys. Fluid.*, **35**, 117127. https://doi.org/10.1063/5.0175412.